

Article

Flexural Capacity of a New Composite Beam with Concrete-Infilled Tubular Lower Flange

Bong-Ho Cho ¹, Jae-Sub Lee ¹, Young-Ho Kim ² and Dae-Jin Kim ^{3,*}

¹ Department of Architectural Engineering, Ajou University, Suwon 16499, Korea; bhcho@ajou.ac.kr (B.-H.C.); jaesubyoyo@ajou.ac.kr (J.-S.L.)

² Institute of R&D, Ji Seung Consultant Co., Ltd., Seoul 03058, Korea; steelkyh@hanmail.net

³ Department of Architectural Engineering, Kyung Hee University, Yongin 17104, Korea

* Correspondence: djkim@khu.ac.kr; Tel.: +82-31-201-3329

Academic Editor: Wen-Hsiang Hsieh

Received: 11 October 2016; Accepted: 18 November 2016; Published: 6 January 2017

Abstract: This paper proposes a new steel concrete composite beam that has a similar shape to the conventional steel wide flange beam, but whose lower flange has a tubular shape with infilled concrete. It has openings in the web for perfect integration between concrete and steel materials, and the tubular lower flange is reinforced with steel rebars to enhance its flexural strength. The bending capacity of the new composite beam was investigated by performing a two-point loading test on seven specimens, which can be categorized mainly into two types, non-composite and fully composite specimens. The load versus displacement curves were plotted for all the specimens and their failure modes were identified. Theoretical equations were proposed to estimate the flexural strength of the new composite beam members, and their accuracy was examined by comparing the predictions of the equations with the test results.

Keywords: composite beam; deep deck; tubular flange; honey comb beam

1. Introduction

It is well known that steel–concrete composite members are structural system that can optimize the mechanical properties and material characteristics of steel and concrete. In addition to the conventional composite members utilizing wide flange shapes and shear studs, various types of steel–concrete composite members have recently been proposed, and their usage has increased on construction sites.

One of the main goals of the recently developed composite systems is the reduction of floor height. ‘Thor-beam’ and ‘Delta-beam’ developed in Scandinavia [1] and the ‘slimflor beam’ by the Steel Construction Institute [2] are representative examples with this feature. These slim floor beams are generally used in conjunction with deep decks and hollow core slabs for 5 m to 9 m span [1–3]. Nardin et al. [4,5] suggested a methodology that can determine the optimal locations of shear connectors by performing a test on several slim floor beam specimens. Lawson et al. [6] proposed a new slim floor beam system without shear connectors that can guarantee a sufficient level of composite action between the two materials and derived its design strength equations. Braun et al. [7,8] developed a composite slim floor beam (CoSFB) that retains an enhanced flexural capacity by utilizing dowel bars passing through the web of the beam section. The typical span of slim floor beams is approximately 8 m, but the maximum span of the CoSFB system can be extended to 14 m while limiting the overall floor depth within 400 mm.

The reduction of the amount of steel material and improved constructability are other goals of recently developed composite systems. The ‘Versa :T:’ beam by Divesakore is one such example; its main concept is that the steel cross section plays the role of a form for concrete and functions as a structural component. Lee et al. [9,10] developed a similar composite beam utilizing high-strength

steel for the improvement of its flexural and seismic capacity. Kim et al. [11,12] developed a new composite beam that includes bolted cold-formed steel components and steel rebars for improved bending strength.

This study proposes a new steel–concrete composite beam system with tubular lower flange illustrated in Figure 1. The composition of its cross-sectional components is shown in Figure 2. This new composite member has openings in the web for perfect integration of the concrete and steel materials, and steel rebars are installed inside the tubular lower flange to enhance its flexural strength. It allows the use of deep decks and piping members passing through the web for floor depth reduction.

In this paper, the bending capacity of the new composite beam is investigated by performing a two-point loading test on seven specimens, which can be categorized mainly into two types, non-composite and fully composite specimens. The load versus displacement curves are plotted for all the specimens and their ultimate failure modes are identified. Theoretical equations to estimate the flexural strengths of the new composite beam members are proposed, and their accuracy is examined by comparing the predictions of the equations with the test results.

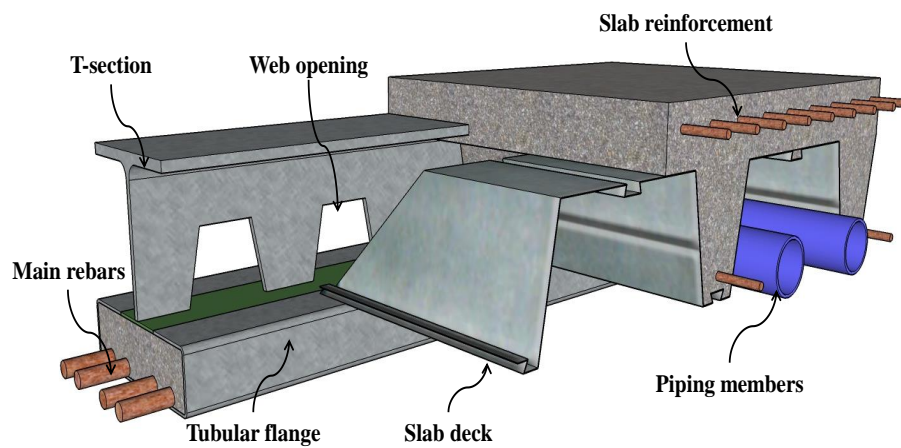


Figure 1. Composite beam system with tubular lower flange.

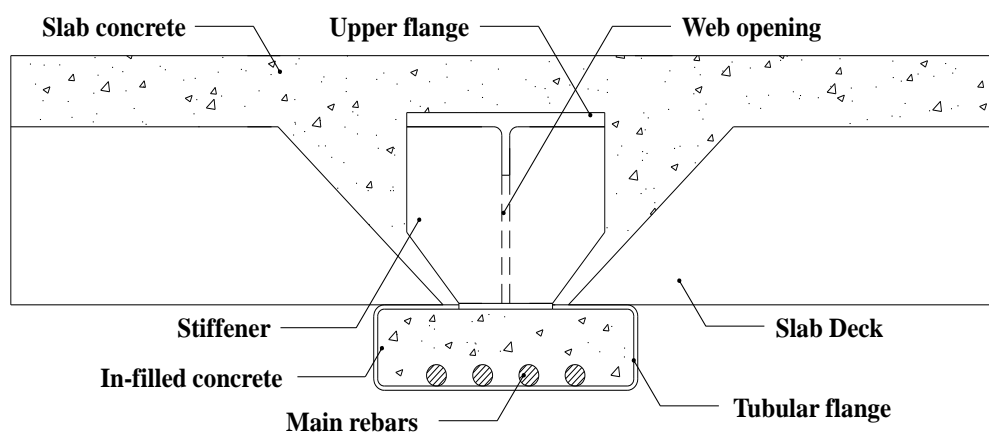


Figure 2. Composite beam section.

2. Experimental Program

2.1. Test Specimens

In this study, a total of seven specimens were manufactured and tested for the evaluation of the flexural strength of the proposed composite beam. Five of them are non-composite beam specimens at construction stage, and the other two are fully composite specimens with floor deck components.

The test parameters of the non-composite beam specimens include the depth of the beam, existence of web openings, and location of main rebars. The conventional wide flange specimen is also added as the reference non-composite specimen for comparison purposes. The two fully composite specimens include the proposed composite beam specimen with deep floor deck and a conventional wide flange specimen with a truss floor deck. In all of the proposed composite beam specimens, its lower tubular flange is reinforced with four D32 rebars. The notation used to indicate each set of test parameters is presented in Figure 3. The details of the seven specimens are summarized in Table 1, and their cross-sectional shapes of the seven specimens are illustrated in Figure 4. All the specimens with web openings have exactly the same opening details as shown in Figure 5.

The compressive strength of concrete (F_{ck}) was measured in accordance with the standards of [13], and the measured average values are summarized in Table 2. Its modulus of elasticity (E_c) is estimated using the following formula provided in [14]:

$$E_c = 8500 \sqrt[3]{F_{cu}}, \tag{1}$$

where F_{cu} is the cube compressive strength of concrete and can be calculated using $F_{cu} = F_{ck} + \Delta F$. If F_{ck} is less than 40 MPa, ΔF is given as 4 MPa. The material properties of steel components of the test specimens are listed in Table 3, which were measured per ASTM A370 [15].

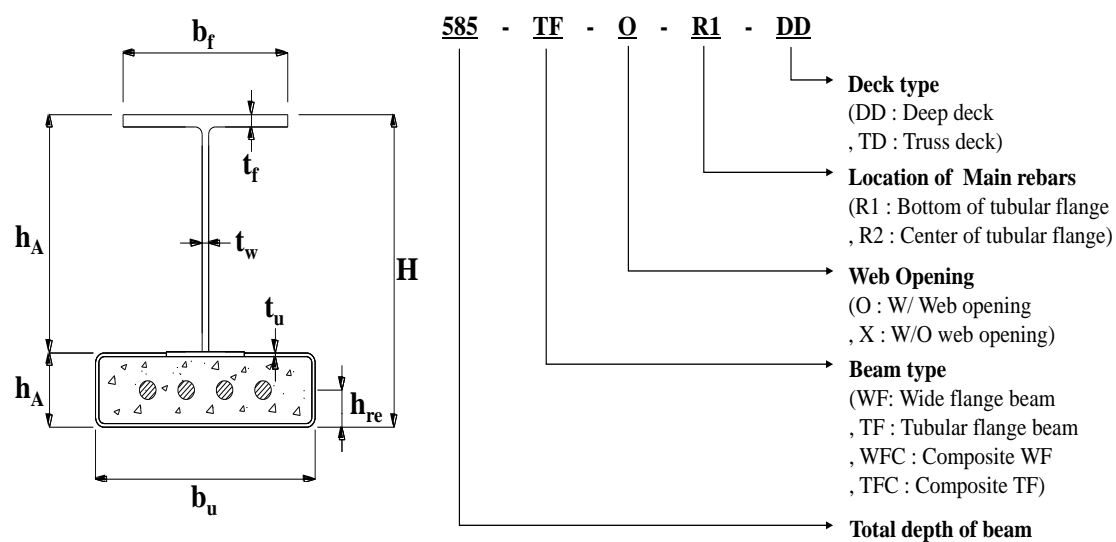


Figure 3. Specimen identification.

Table 1. Details of test specimens.

Specimen	Type of Specimen	Steel Beam Depth (mm)	Existence of Web Openings	Location of Main Rebars	Type of Floor Deck	
588-WF-X	Non-composite	588	No	N/A	N/A	
505-TF-X-R1						
505-TF-O-R1						Bottom
505-TF-O-R2						Middle
390-TF-O-R1						Bottom
738-WFC-X-X-TD	Fully composite	588	No	N/A	Truss deck	
585-TFC-O-R1-DD						Bottom

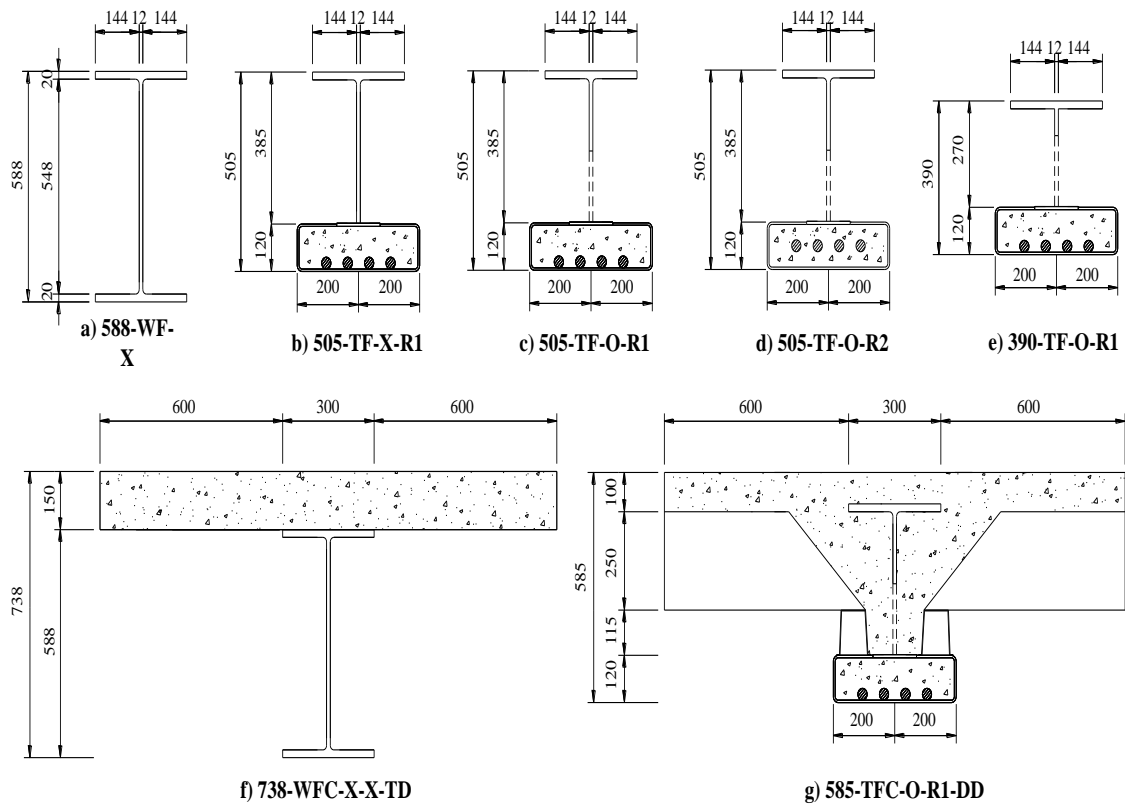


Figure 4. Cross-sectional shapes of test specimens.

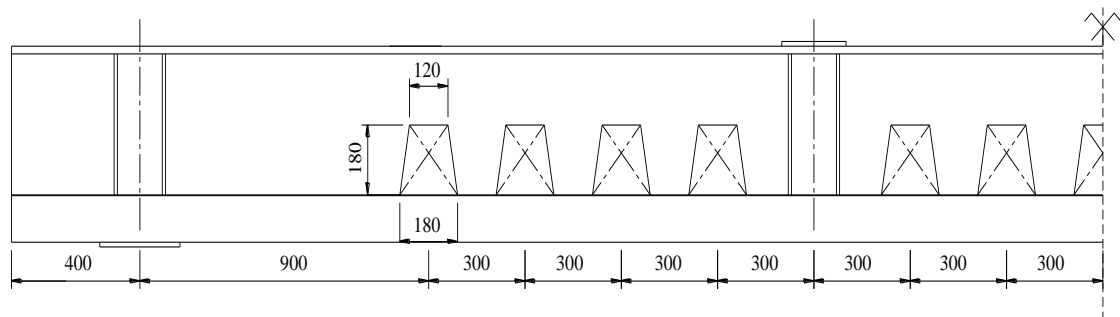


Figure 5. Web opening details of test specimens.

Table 2. Concrete material properties (unit: N/mm²).

Concrete Type	Compressive Strength	Modulus of Elasticity
Tube infilled concrete	29.8	27,474.5
Slab deck concrete	29.4	27,360.1

Table 3. Material properties of steel components (units: N/mm², $\mu\text{m}/\text{m}$).

Component	Yield Strength	Ultimate Strength	Yield Strain
Upper flange	328.3	513.3	1561.4
Web	399.9	541.6	1844.9
Lower tubular flange	456.5	537.6	1991.8
Main rebars	548.6	698.2	2676.2

2.2. Test Setup

The schematic drawings of the test setup for the non-composite and fully composite specimens are illustrated in Figure 6a,b, respectively. In all of the test specimens, the length of the span is 6 m, and the distance from the loading point to the support is 2.1 m. Load was applied to each specimen at a rate of 15 kN/min using a hydraulic cylinder with a maximum capacity of 1000 kN. The force generated by the hydraulic cylinder was transmitted to the center of a steel frame, which was installed to apply a two-point loading to the beam specimen. The distance between the two loading points is 1800 mm. The magnitude of the loading was measured by a load cell attached to the bottom of the cylinder, and the vertical displacement was monitored by a linear variable differential transducer (LVDT) installed at the midspan of the beam. A number of strain gauges were attached in the region near the span center as shown in the figure. The locations of the strain gauges for the non-composite and fully composite specimens are illustrated in Figure 7a,b, respectively. The data measured by the strain gauges at each loading stage are utilized to identify the location of the neutral axis, as discussed in Section 4. A photo of the actual test setup is given in Figure 8.

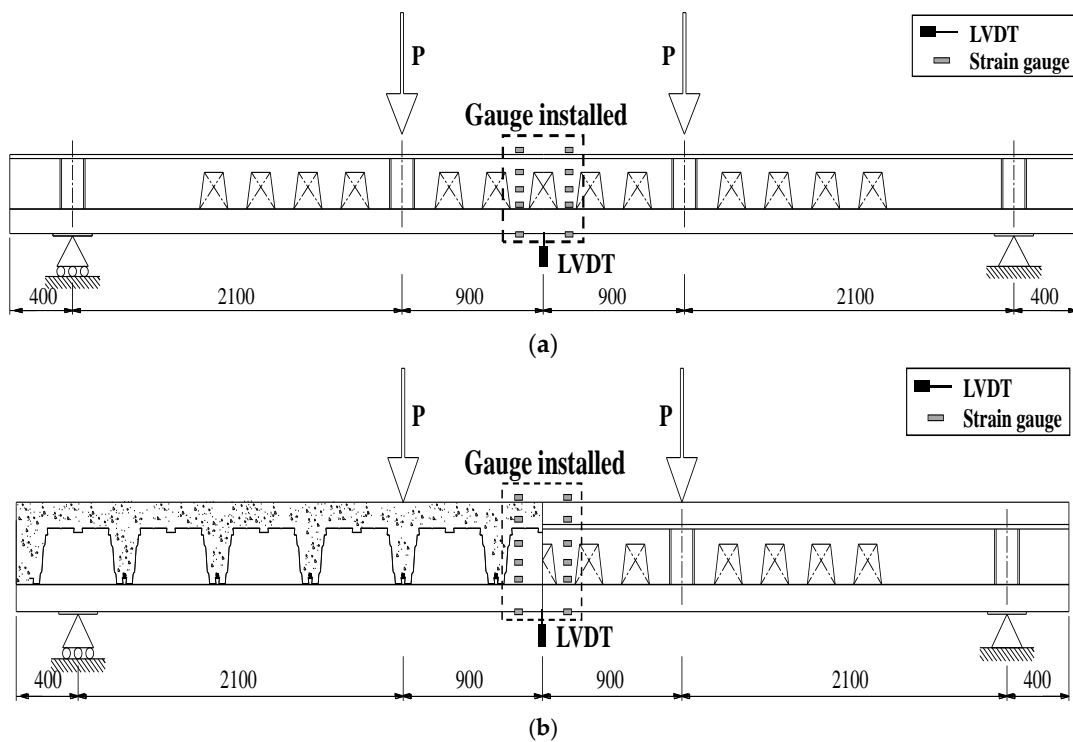


Figure 6. Schematic test setup: (a) non-composite specimens; (b) fully composite specimens.

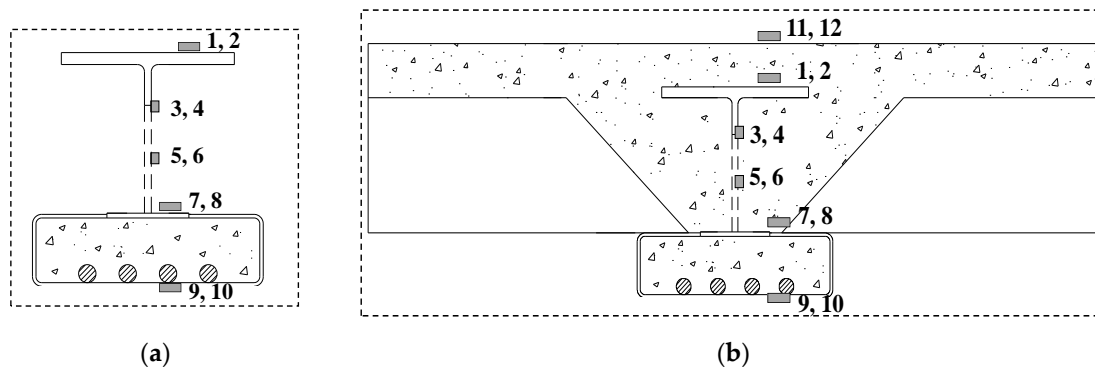


Figure 7. Strain gauge locations: (a) non-composite specimens; (b) fully composite specimens.



Figure 8. Photo of the actual test setup.

3. Flexural Strength Estimation

3.1. Non-Composite Specimens

In this section, the nominal flexural strength equations of the non-composite specimens at construction stage are derived for two different cases, depending on the existence of openings in the web. If no openings exist in the web, it is suggested that the smaller of the plastic moment (M_p) and lateral torsional moment (M_{LTB}) of the given construction stage section is taken as the nominal flexural strength (M_n), as in the design of conventional wide flange sections. However, if openings exist in the web, its yield moment (M_y) is taken as the nominal flexural strength. This is mainly because the ultimate failure mode of the non-composite specimens is generally the local web buckling, as discussed in Section 4.1. Similarly to this case, the Load and Resistance Factors Design (LRFD) of the American Institute of Steel Construction (AISC) [16] recommends that the nominal flexural strength of the composite beam section with noncompact web shape should be estimated based on its yield moment. The test results in Section 4.1 confirm that this approach can accurately predict the flexural strengths of the non-composite beams with web openings. It is assumed that the non-composite specimens considered in this study satisfy the width/thickness ratio criteria provided in the LRFD design specification for its upper flange and web components.

Figure 9 illustrates the three representative locations of the plastic neutral axis (PNA) for the non-composite beam sections without web openings. The plastic moment estimation for these three cases can be straightforwardly done as follows.

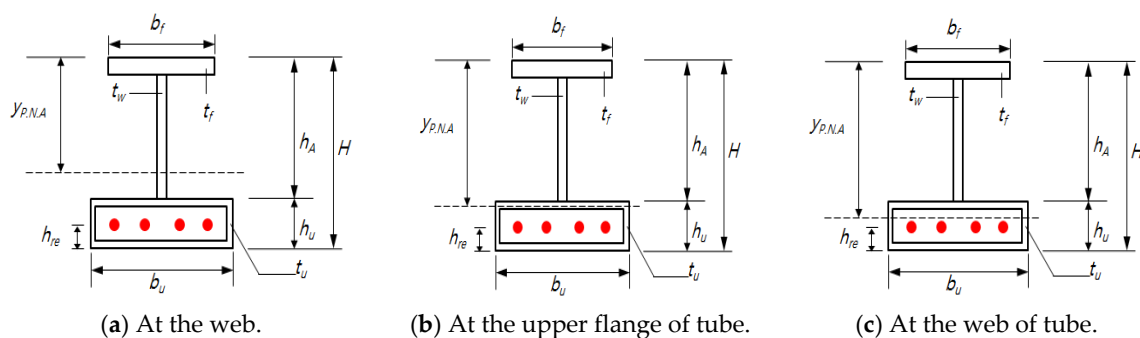


Figure 9. Locations of plastic neutral axis for the non-composite specimen without web openings.

(1) In case the plastic neutral axis exists at the web

The internal axial force for each component of the section can be computed as shown in Table 4. In the equations of the table, F_y and $F_{y,re}$ represent the yield strengths of steel plate components and rebars, respectively. In addition, n and A_{re} denote the number of rebars used and the area of a single rebar, respectively. It is assumed that the contribution of concrete components subjected to tension force is ignored. The location of the PNA (y_{PNA}) for this case can be determined from the axial force equilibrium condition expressed below:

$$C_{Af} + C_{Aw} = T_{Aw} + T_{tuf} + T_{tw} + T_{tbf} + T_{re}. \tag{2}$$

By using the PNA location determined from the above equation, the plastic moment of the given composite section can be calculated by:

$$M_p = C_{Af} \times (y_{PNA} - \frac{t_f}{2}) + C_{Aw} \times \frac{(y_{PNA} - t_f)}{2} + T_{Aw} \times \frac{(h_A - y_{PNA})}{2} + T_{tuf} \times (h_A - y_{PNA} + \frac{t_u}{2}) + T_{tw} \times (h_A - y_{PNA} + \frac{h_u}{2}) + T_{tbf} \times (H - y_{PNA} - \frac{t_u}{2}) + T_{re} \times (H - y_{PNA} - h_{re}) \tag{3}$$

Table 4. Internal force components in case the plastic neutral axis exists at the web.

Internal Axial Force Component	Force Equation
Compression force at upper flange (C_{Af})	$C_{Af} = b_f \times t_f \times F_y$
Compression force at web above PNA (C_{Aw})	$C_{Aw} = t_w \times (y_{PNA} - t_f) \times F_y$
Tension force at web below PNA (T_{Aw})	$T_{Aw} = t_w \times (h_A - y_{PNA}) \times F_y$
Tension force at upper flange of tube (T_{tuf})	$T_{tuf} = b_u \times t_u \times F_y$
Tension force at web of tube (T_{tw})	$T_{tw} = 2t_u \times (h_u - 2t_u) \times F_y$
Tension force at lower flange of tube (T_{tbf})	$T_{tbf} = b_u \times t_u \times F_y$
Tension force at main rebars (T_{re})	$T_{re} = n \times A_{re} \times F_{y,re}$

(2) In case the plastic neutral axis exists at the upper flange of the tube

The internal axial force for each component of the section can be computed as shown in Table 5. The location of the PNA for this case can be determined from the axial force equilibrium condition expressed below:

$$C_{Af} + C_{Aw} + C_{tuf} = T_{tuf} + T_{tw} + T_{tbf} + T_{re}. \tag{4}$$

By using the PNA location determined from the above equation, the plastic moment of the given composite section can be calculated by:

$$M_p = C_{Af} \times (y_{PNA} - \frac{t_f}{2}) + C_{Aw} \times (y_{PNA} - t_f - \frac{(h_A - t_f)}{2}) + C_{tuf} \times \frac{(y_{PNA} - h_A)}{2} + T_{tuf} \times (\frac{h_A + t_u - y_{PNA}}{2}) + T_{tw} \times (h_A - y_{PNA} + \frac{h_u}{2}) + T_{tbf} \times (H - y_{PNA} - \frac{t_u}{2}) + T_{re} \times (H - y_{PNA} - h_{re}) \tag{5}$$

Table 5. Internal force components in case the plastic neutral axis exists at the upper flange of the tube.

Internal Axial Force Component	Force Equation
Compression force at upper flange (C_{Af})	$C_{Af} = b_f \times t_f \times F_y$
Compression force at web (C_{Aw})	$C_{Aw} = t_w \times (h_A - t_f) \times F_y$
Compression force at upper flange of tube above PNA (C_{tuf})	$C_{tuf} = b_u \times (y_{PNA} - h_A) \times F_y$
Tension force at upper flange of tube below PNA (T_{tuf})	$T_{tuf} = b_u \times (h_A + t_u - y_{PNA}) \times F_y$
Tension force at web of tube (T_{tw})	$T_{tw} = 2t_u \times (h_u - 2t_u) \times F_y$
Tension force at lower flange of tube (T_{tbf})	$T_{tbf} = b_u \times t_u \times F_y$
Tension force at main rebars (T_{re})	$T_{re} = n \times A_{re} \times F_{y,re}$

(3) In case the plastic neutral axis exists at the web of the tube

The internal axial force for each component of the section can be computed as shown in Table 6. It is assumed that the contribution of all concrete components to the flexural strength of the member is ignored because only a small portion of concrete is subjected to compression force, as shown in Figure 9c. The location of the PNA for this case can be determined from the axial force equilibrium condition expressed below:

$$C_{Af} + C_{Aw} + C_{tuf} + C_{tw} = T_{tw} + T_{tbf} + T_{re}. \tag{6}$$

By using the PNA location determined from the above equation, the plastic moment of the given composite section can be calculated by:

$$M_p = C_{Af} \times (y_{PNA} - \frac{t_f}{2}) + C_{Aw} \times (y_{PNA} - t_f - \frac{(h_A - t_f)}{2}) + C_{tuf} \times (y_{PNA} - h_A - \frac{t_u}{2}) + C_{tw} \times (\frac{y_{PNA} - h_A - t_u}{2}) + T_{tw} \times (\frac{H - y_{PNA} - t_u}{2}) + T_{tbf} \times (H - y_{PNA} - \frac{t_u}{2}) + T_{re} \times (H - y_{PNA} - h_{re}) \tag{7}$$

Table 6. Internal force components in case the plastic neutral axis exists at the web of the tube.

Internal Axial Force Component	Force Equation
Compression force at upper flange (C_{Af})	$C_{Af} = b_f \times t_f \times F_y$
Compression force at web (C_{Aw})	$C_{Aw} = t_w \times (h_A - t_f) \times F_y$
Compression force at upper flange of tube (C_{tuf})	$C_{tuf} = b_u \times t_u \times F_y$
Compression force at web of tube above PNA (C_{tw})	$C_{tw} = 2t_u \times (y_{PNA} - h_A - t_u) \times F_y$
Tension force at web of tube below PNA (T_{tw})	$T_{tw} = 2t_u \times (H - y_{PNA} - t_u) \times F_y$
Tension force at lower flange of tube (T_{tbf})	$T_{tbf} = b_u \times t_u \times F_y$
Tension force at main rebars (T_{re})	$T_{re} = n \times A_{re} \times F_{y,re}$

The lateral torsional moment of the non-composite beam sections can be calculated by following the procedure introduced in the LRFD specification. Since the composite beam proposed in this study has a different cross-sectional shape from the conventional wide flange sections, the warping constant (C_w) and torsional constant (J) need to be evaluated by the following equations:

$$C_w = a^2 I_1 + b^2 I_2, \tag{8}$$

$$J = \frac{b_f t_f^3}{3} + \frac{4 \times A_p^2}{p/t_u}, \tag{9}$$

where several new variables in the above equations can be computed by

$$I_1 = \frac{t_f \times b_f^3}{12}, I_2 = 2 \times (\frac{t_u b_u^3}{12} + \frac{h_u t_u^3}{12} + t_u h_u \times (\frac{b_u}{2} - \frac{t_u}{2})^2) + 2 \times (\frac{\pi \times r_{re}^4}{2} + \pi \times r_{re}^2 \times ((\frac{b_u}{8})^2 + (\frac{3 \times b_u}{8})^2)),$$

$$\rho = \frac{I_1}{I_1 + I_2}, a = (1 - \rho) \times (H - \frac{t_f}{2} - \frac{h_u}{2}), b = \rho \times (H - \frac{t_u}{2} - \frac{h_u}{2}),$$

$$A_p = (b_u - t_u) \times (h_u - t_u), p = 2 \times ((b_u - t_u) + (h_u - t_u)).$$

The yield moment of the non-composite beam section with web openings illustrated in Figure 10 can be computed by determining the location of the elastic neutral axis (y_{NA}) as follows:

$$y_{NA} = \frac{\sum A \bar{y}}{\sum A}, \tag{10}$$

where

$$\begin{aligned} \sum A\bar{y} &= b_f t_f \times \frac{t_f}{2} + t_w (h_A - t_f - h_h) \times \frac{(h_A + t_f - h_h)}{2} + b_u t_u \times (h_A + \frac{t_u}{2}) + 2(h_u - 2t_u)t_u \times (h_A + \frac{h_u}{2}) \\ &\quad + b_u t_u \times (H - \frac{t_u}{2}) + n A_{re} \times (H - h_{re}), \\ \text{and } \sum A &= b_f t_f + t_w (h_A - t_f - h_h) + 2b_u t_u + 2(h_u - 2t_u)t_u + n A_{re}. \end{aligned}$$

From this equation, the moment of inertia of the entire composite section (I_T) can be written as:

$$\begin{aligned} I_T &= \frac{b_f t_f^3}{12} + b_f t_f \times (y_{NA} - \frac{t_f}{2})^2 + \frac{t_w (h_A - t_f - h_h)^3}{12} + t_w (h_A - t_f - h_h) \times (y_{NA} - \frac{h_A + t_f - h_h}{2})^2 \\ &\quad + \frac{b_u t_u^3}{12} + b_u t_u \times (y_{NA} - h_A - \frac{t_u}{2})^2 + 2 \times (\frac{t_u (h_u - 2t_u)^3}{12} + (h_u - 2t_u)t_u \times (y_{NA} - h_A - \frac{h_u}{2})^2) \cdot \quad (11) \\ &\quad + \frac{b_u t_u^3}{12} + b_u t_u \times (y_{NA} - H + \frac{t_u}{2})^2 + n \times (\frac{\pi \times r_{re}^4}{4} + \pi \times r_{re}^2 \times (H - h_{re})^2) \end{aligned}$$

Finally, the yield moment can be expressed as:

$$M_y = \frac{F_y I_T}{y_{\max}}, \quad (12)$$

where y_{\max} is the larger of the distances from the elastic neutral axis to the top and bottom of the section. In the derivation of Equation (12), it is assumed that the rebars have a higher yield strength than that of steel plate components, thus yielding first occurs at the top or bottom fiber of the section.

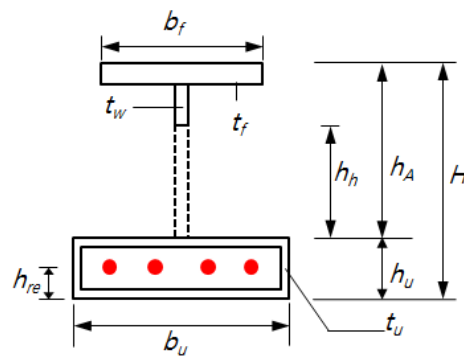


Figure 10. Cross-sectional shape of the non-composite beam with web openings.

3.2. Fully Composite Specimens

This section presents the nominal flexural strength equations of the fully composite beam with floor deck components. Since the concrete and steel components of the fully composite specimens can be integrated into a single unity due to the existence of the web openings, its plastic moment can be taken as the nominal flexural strength, as discussed in Section 4.2. Figure 11 illustrates the three representative locations of the plastic neutral axis for this section without web openings. As in the LRFD specification, the effective width of slab concrete can be determined as the smaller of the distance between the centers of adjacent slabs and span length if slabs exist on both sides of the composite beam. The plastic moments for the three cases can be straightforwardly calculated as follows.

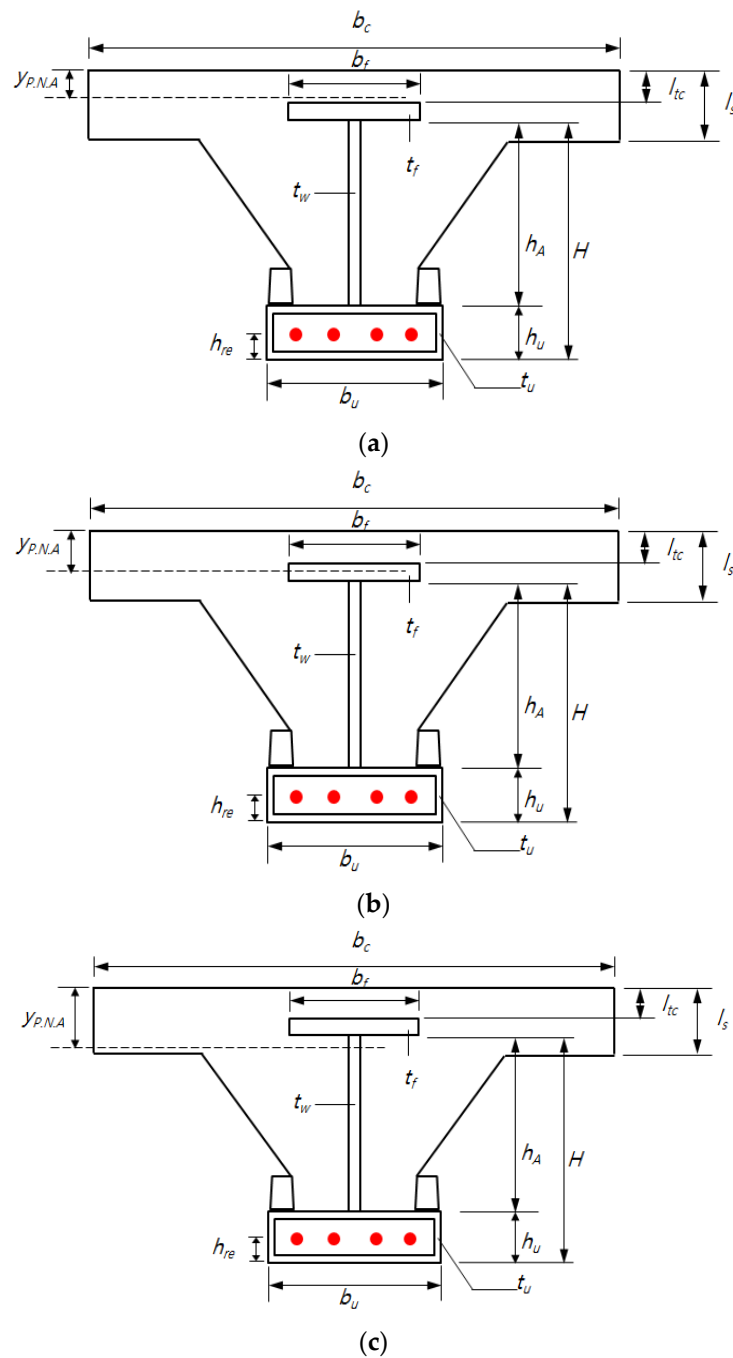


Figure 11. Locations of plastic neutral axis for the fully composite specimen: (a) above the upper flange; (b) at the upper flange; (c) below the upper flange.

(1) In case the plastic neutral axis exists above the upper flange

The internal axial force for each component of the section can be computed as shown in Table 7. In the equations of the table, F_{ck} is the compressive strength of concrete. It is assumed that the contribution of concrete components subjected to tension force is ignored. The location of the PNA (y_{PNA}) for this case can be determined from the axial force equilibrium condition expressed below:

$$C_{conc} = T_{Af} + T_{Aw} + T_{tuf} + T_{tuw} + T_{tbf} + T_{re}. \tag{13}$$

By using the PNA location determined from the above equation, the plastic moment of the given composite section can be calculated by:

$$M_p = C_{conc} \times \left(\frac{y_{PNA}}{2}\right) + T_{Af} \times \left(l_{tc} - y_{PNA} + \frac{t_u}{2}\right) + T_{Aw} \times \left(l_{tc} - y_{PNA} + t_f + \frac{h_A}{2}\right) + T_{tuf} \times \left(l_{tc} - y_{PNA} + t_f + h_A + \frac{t_u}{2}\right) + T_{tw} \times \left(l_{tc} - y_{PNA} + t_f + h_A + \frac{h_u}{2}\right) + T_{tbf} \times \left(l_{tc} - y_{PNA} + t_f + H - \frac{t_u}{2}\right) + T_{re} \times \left(l_{tc} - y_{PNA} + t_f + H - h_{re}\right) \quad (14)$$

Table 7. Internal force components in case the plastic neutral axis exists above the upper flange.

Internal Axial Force Component	Force Equation
Concrete compression force above PNA (C_{conc})	$C_{conc} = b_c \times y_{PNA} \times 0.85F_{ck}$
Tension force at upper flange (T_{Af})	$T_{Af} = b_f \times t_f \times F_y$
Tension force at web (T_{Aw})	$T_{Aw} = h_A \times t_w \times F_y$
Tension force at upper flange of tube (T_{tuf})	$T_{tuf} = b_u \times t_u \times F_y$
Tension force at web of tube (T_{tw})	$T_{tw} = 2t_u \times (h_u - 2t_u) \times F_y$
Tension force at lower flange of tube (T_{tbf})	$T_{tbf} = b_u \times t_u \times F_y$
Tension force at main rebars (T_{re})	$T_{re} = n \times A_{re} \times F_{y,re}$

(2) In case the plastic neutral axis exists at the upper flange

The internal axial force for each component of the section can be computed as shown in Table 8. The location of the PNA for this case can be determined from the axial force equilibrium condition expressed below:

$$C_{conc} + C_{Af} = T_{Af} + T_{Aw} + T_{tuf} + T_{tw} + T_{tbf} + T_{re} \quad (15)$$

By using the PNA location determined from the above equation, the plastic moment of the given composite section can be calculated by:

$$M_p = C_{conc} \times \left(\frac{y_{PNA}}{2}\right) + C_{Af} \times \left(\frac{y_{PNA} - l_{tc}}{2}\right) + T_{Af} \times \left(\frac{l_{tc} + t_f - y_{PNA}}{2}\right) + T_{Aw} \times \left(l_{tc} - y_{PNA} + t_f + \frac{h_A}{2}\right) + T_{tuf} \times \left(l_{tc} - y_{PNA} + t_f + h_A + \frac{t_u}{2}\right) + T_{tw} \times \left(l_{tc} - y_{PNA} + t_f + h_A + \frac{h_u}{2}\right) + T_{tbf} \times \left(l_{tc} - y_{PNA} + t_f + H - \frac{t_u}{2}\right) + T_{re} \times \left(l_{tc} - y_{PNA} + t_f + H - h_{re}\right) \quad (16)$$

Table 8. Internal force components in case the plastic neutral axis exists at the web.

Internal Axial Force Component	Force Equation
Concrete compression force above PNA (C_{conc})	$C_{conc} = b_c \times y_{PNA} \times 0.85F_{ck}$
Compression force at upper flange above PNA (C_{Af})	$C_{Af} = b_f \times (y_{PNA} - l_{tc}) \times F_y$
Tension force at upper flange below PNA (T_{Af})	$T_{Af} = b_f \times (l_{tc} + t_f - y_{PNA}) \times F_y$
Tension force at web (T_{Aw})	$T_{Aw} = h_A \times t_w \times F_y$
Tension force at upper flange of tube (T_{tuf})	$T_{tuf} = b_u \times t_u \times F_y$
Tension force at web of tube (T_{tw})	$T_{tw} = 2t_u \times (h_u - 2t_u) \times F_y$
Tension force at lower flange of tube (T_{tbf})	$T_{tbf} = b_u \times t_u \times F_y$
Tension force at main rebars (T_{re})	$T_{re} = n \times A_{re} \times F_{y,re}$

(3) In case the plastic neutral axis exists below the upper flange

The internal axial force for each component of the section can be computed as shown in Table 9. The location of the PNA for this case can be determined from the axial force equilibrium condition expressed below:

$$C_{conc} + C_{Af} + C_{Aw} = T_{Aw} + T_{tuf} + T_{tw} + T_{tbf} + T_{re} \quad (17)$$

By using the PNA location determined from the above equation, the plastic moment of the given composite section can be calculated by:

$$M_p = C_{conc} \times \left(\frac{y_{PNA}}{2}\right) + C_{Af} \times (y_{PNA} - l_{tc} - \frac{t_f}{2}) + C_{Aw} \times \left(\frac{y_{PNA} - l_{tc} - t_f}{2}\right) + T_{Aw} \times \left(\frac{l_{tc} + t_f + h_A - y_{PNA}}{2}\right) + T_{tuf} \times (l_{tc} - y_{PNA} + t_f + h_A + \frac{t_u}{2}) + T_{tw} \times (l_{tc} - y_{PNA} + t_f + h_A + \frac{h_u}{2}) + T_{tbf} \times (l_{tc} - y_{PNA} + t_f + H - \frac{t_u}{2}) + T_{re} \times (l_{tc} - y_{PNA} + t_f + H - h_{re}) \quad (18)$$

Table 9. Internal force components in case the plastic neutral axis exists below the upper flange.

Internal Axial Force Component	Force Equation
Concrete compression force above PNA (C_{conc})	$C_{conc} = b_c \times y_{PNA} \times 0.85F_{ck}$
Compression force at upper flange (C_{Af})	$C_{Af} = b_f \times t_f \times F_y$
Compression force at web above PNA (C_{Aw})	$C_{Aw} = t_w \times (y_{PNA} - l_{tc} - t_f) \times F_y$
Tension force at web below PNA (T_{Aw})	$T_{Aw} = t_w \times (l_{tc} + t_f + h_A - y_{PNA}) \times F_y$
Tension force at upper flange of tube (T_{tuf})	$T_{tuf} = b_u \times t_u \times F_y$
Tension force at web of tube (T_{tw})	$T_{tw} = 2t_u \times (h_u - 2t_u) \times F_y$
Tension force at lower flange of tube (T_{tbf})	$T_{tbf} = b_u \times t_u \times F_y$
Tension force at main rebars (T_{re})	$T_{re} = n \times A_{re} \times F_{y,re}$

4. Test Results and Discussion

4.1. Non-Composite Specimens

Table 10 summarizes the flexural strengths of the five non-composite specimens by the theoretical estimation and test and their ultimate failure modes. Their nominal flexural strengths are estimated using the strength equations provided in Section 3.1. In order to take into account the effect of the self-weight of the specimens on the test results, the adjusted nominal flexural strengths are calculated by subtracting the moment by the self-weight from the nominal flexural strengths. These are in turn compared with the maximum moments obtained from the test results, and the ratios of the latter to the former are also provided in the table. In Figure 12, the load versus displacement curves of the five specimens are presented, and the peak load point of each curve is represented by an empty circle. The photos showing the ultimate failure mode of each specimen are given in Figure 13.

Table 10. Test results of the non-composite specimens.

Specimen	Theoretical Estimation (kN·m)			Test Results (kN·m)		Ratio of (2) to (1) (%)
	Nominal Flexural Strength	Moment by Self-Weight	Adjusted Nominal Flexural Strength ⁽¹⁾	Maximum Moment ⁽²⁾	Ultimate Failure Mode	
588-WF-X	1479.2	6.5	1472.7	1806.5	Bending failure + Local flange buckling	122.7
505-TF-X-R1	1397.3	10.0	1387.3	1660.3	Bending failure + Local flange buckling	119.7
505-TF-O-R1	1052.0	9.7	1042.3	1256.3	Web local buckling	120.5
505-TF-O-R2	977.0	9.7	967.3	1191.0	Web local buckling	123.1
390-TF-O-R1	744.5	9.2	735.3	858.3	Web local buckling	116.7

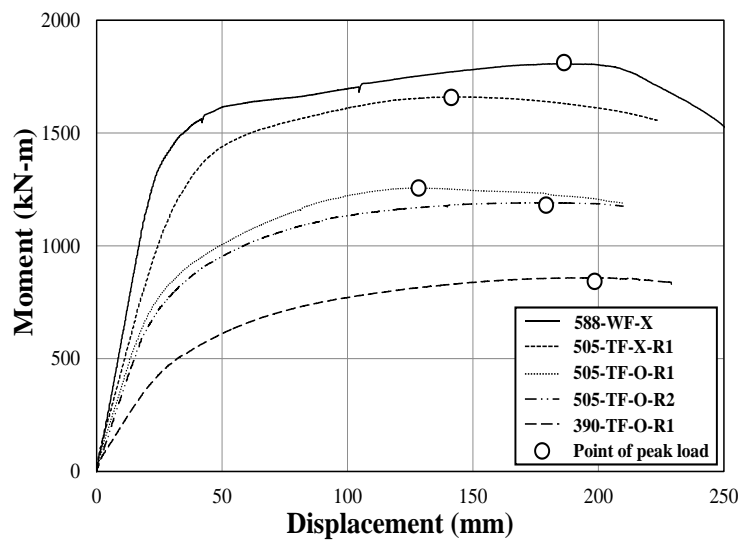


Figure 12. Load versus displacement curves of the non-composite specimens.

It can be noted from these results that the ultimate failure modes of the non-composite specimens without web openings are mainly characterized by bending failure, while those of the non-composite specimens with web openings are mainly characterized by web local buckling failure. This justifies the theoretical flexural strength estimations of Section 3.1, where the flexural strengths of the non-composite specimens without and with web openings are based on the plastic and yield moments, respectively. The ratios of the experimental and theoretical flexural strengths of the specimens ranges from approximately 117% to 123%, which confirms the effectiveness of the strength equations derived in Section 3.1. In addition, it can be seen that the proposed non-composite beam section is highly resistant to lateral torsional buckling due to the existence of its lower tubular flange since no lateral torsional buckling failure occurred in the test specimens.

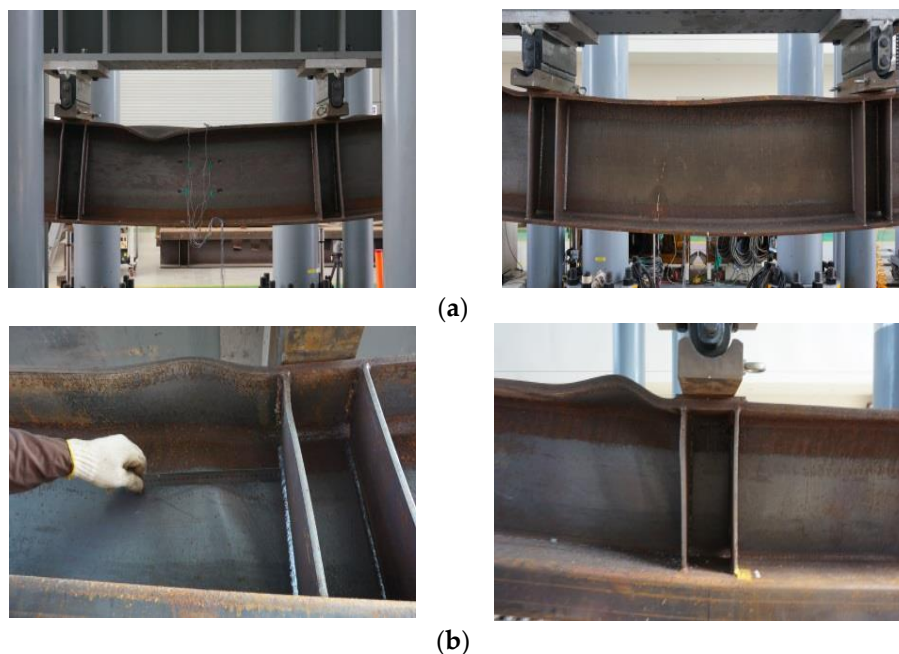


Figure 13. Cont.

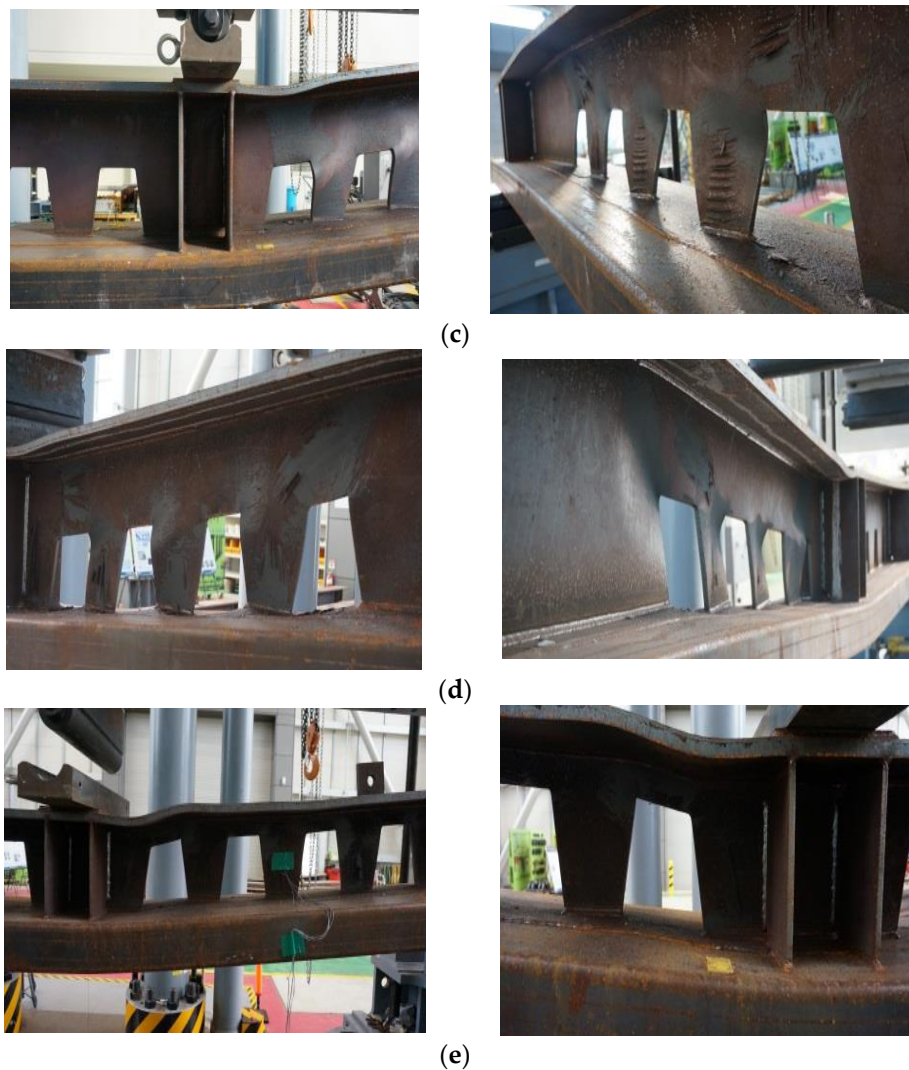


Figure 13. Ultimate failure modes of the non-composite specimens: (a) 588-WF-X; (b) 505-TF-X-R1; (c) 505-TF-O-R1; (d) 505-TF-O-R2; (e) 390-TF-O-R1.

Figure 14 displays the normal strain distributions at span center of the five non-composite specimens at several different loading stages, which correspond to the measured vertical displacements of 10 mm, 20 mm, and 50 mm and at peak load, respectively. The locations of neutral axes at failure by the test result and theoretical estimation of Section 3.1 are listed in Table 11 and also indicated in the figure. The results in the table indicate that their ratios range from approximately 87% to 111%, which confirms that the theoretical estimation is able to accurately predict the location of neutral axis at failure as well.

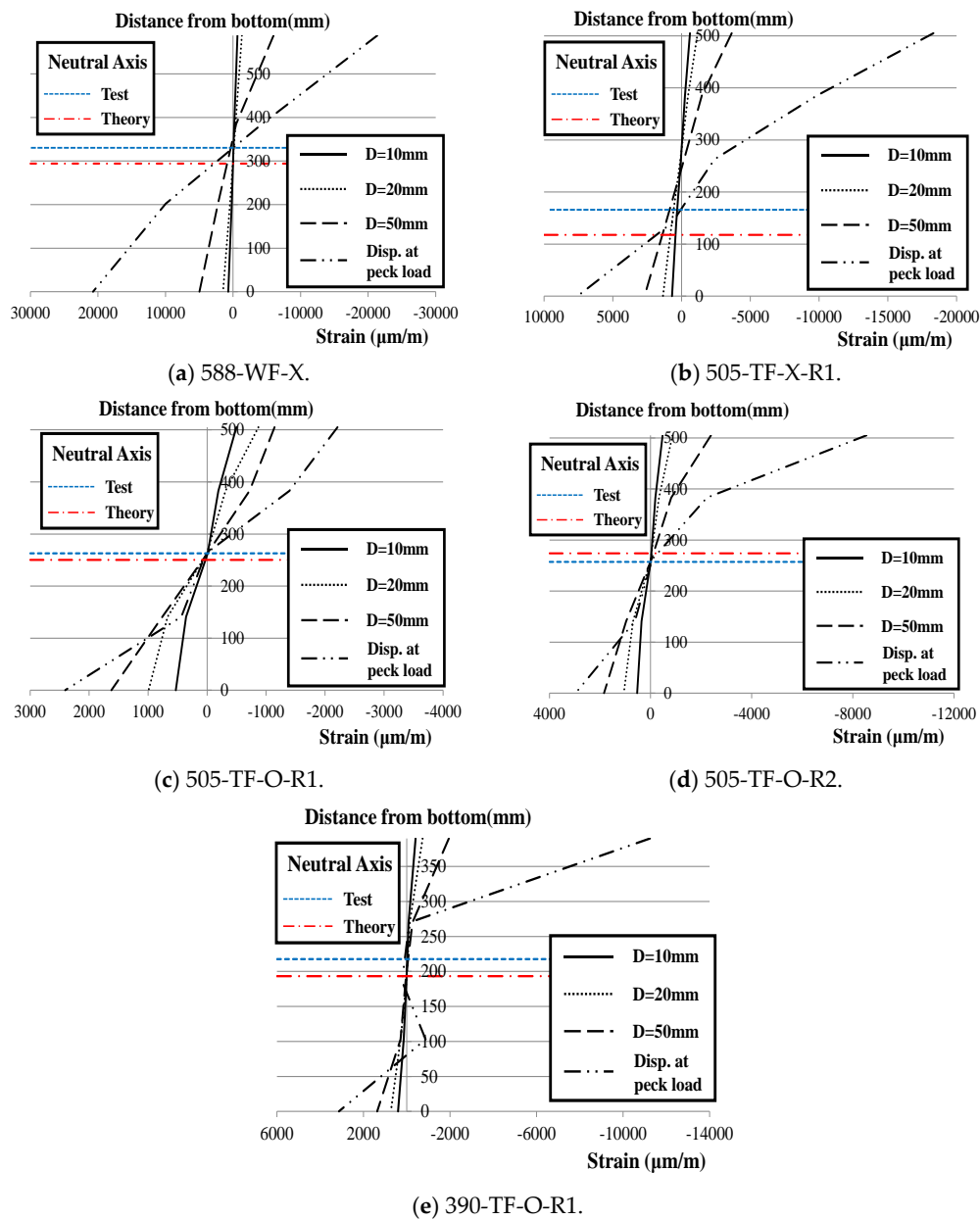


Figure 14. Measured strain distributions of the non-composite specimens.

Table 11. Locations of neutral axis at failure of the non-composite specimens.

Specimen	Location of Neutral Axis at Failure (mm)		Ratio of (2) to (1) (%)
	Theory ⁽¹⁾	Test ⁽²⁾	
588-WF-X	294.0	272.4	92.7
505-TF-X-R1	387.3	335.9	86.7
505-TF-O-R1	254.7	261.0	102.5
505-TF-O-R2	247.7	273.9	110.6
390-TF-O-R1	196.8	172.3	87.6

4.2. Fully Composite Specimens

Similar to the case of the non-composite specimens in Section 4.1, Table 12 summarizes the flexural strengths of the two fully composite specimens by theoretical estimation and testing and their ultimate failure modes. Their nominal flexural strengths are calculated using the strength equations provided in

Section 3.2. Figure 15 plots the load versus displacement curves of the two fully composite specimens, and the ultimate failure mode of each specimen is shown in Figure 16.

These results indicate that the ultimate failure mode of the reference specimen (738-WFC-X-X-TD) is bending failure, while that of the composite specimen with lower tubular flange (585-TFC-O-R1-DD) is premature concrete crushing in the region of the loading point. However, as can be seen from the trend of the load–displacement curve in Figure 15, it is expected that the experimental flexural strength of specimen 585-TFC-O-R1-DD would have been much higher if the region near the loading point of the specimen had been properly reinforced to prevent the premature concrete bearing failure. In addition, it can be emphasized that the experimental flexural strengths of the two specimens do not show much difference, although the reference specimen with the conventional wide flange section has an almost 26% higher total depth than that of the composite specimen with lower tubular flange proposed in this study.

Figure 17 presents the normal strain distributions at the span center of the two fully composite specimens. The locations of neutral axes at peak load by the test result and theoretical estimation of Section 3.2 are listed in Table 13. These results indicate that the neutral axis locations by the test and theory coincide well with each other in the case of the reference specimen, but they do not in the fully composite specimen with tubular lower flange. This seems to happen because the cross section of the latter did not fully yield at the peak load level.

Table 12. Test results of the fully composite specimens.

Specimen	Theoretical Estimation (kN·m)			Test Results (kN·m)		Ratio of (2) to (1) (%)
	Nominal Flexural Strength	Moment by Self-Weight	Adjusted Nominal Flexural Strength ⁽¹⁾	Maximum Moment ⁽²⁾	Ultimate Failure Mode	
738-WFC-X-X-TD	2350.1	31.4	2318.7	2496.0	Bending failure	107.6
585-TFC-O-R1-DD	2288.2	42.1	2246.1	2138.6	Concrete bearing failure	95.2

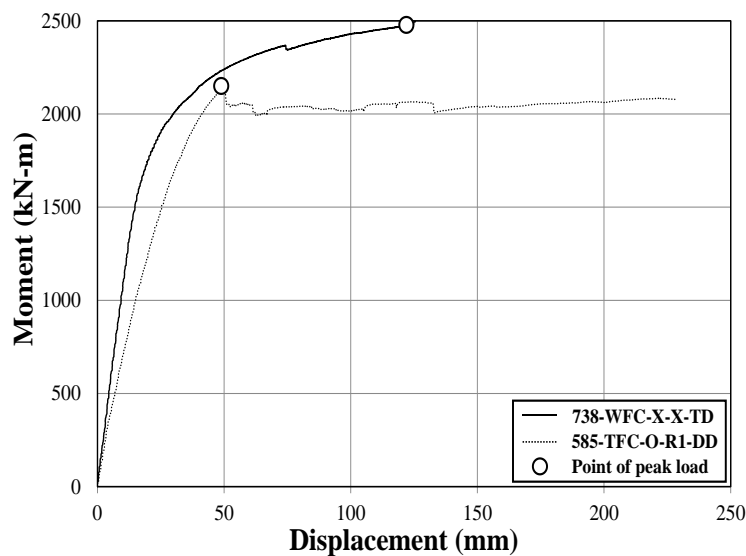


Figure 15. Load versus displacement curves of the fully composite specimens.

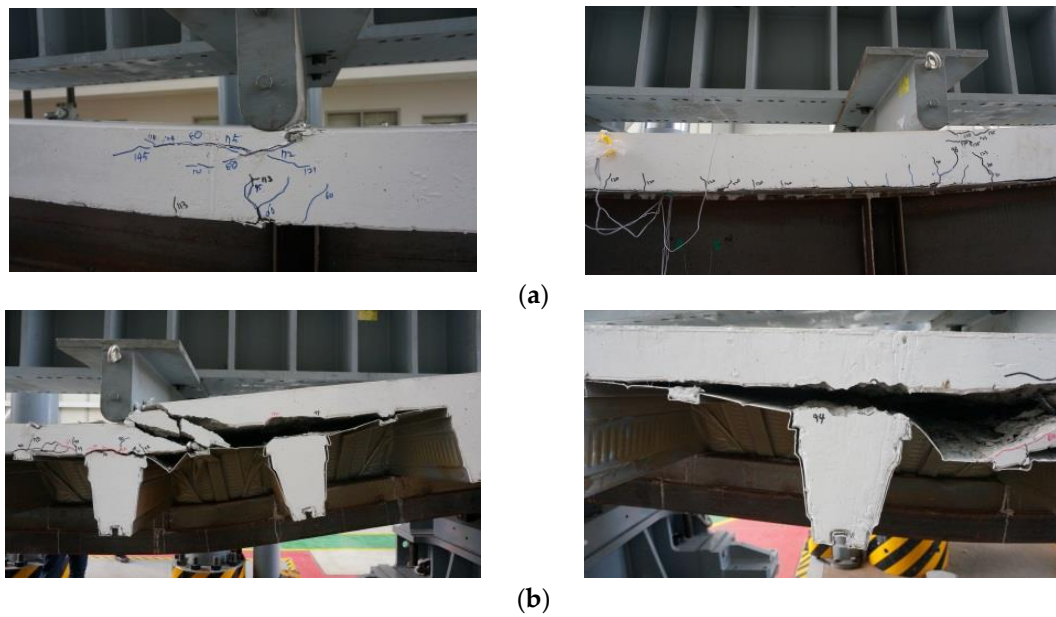


Figure 16. Ultimate failure modes of the fully composite specimens: (a) 738-WFC-X-X-TD; (b) 585-TFC-O-R1-DD.

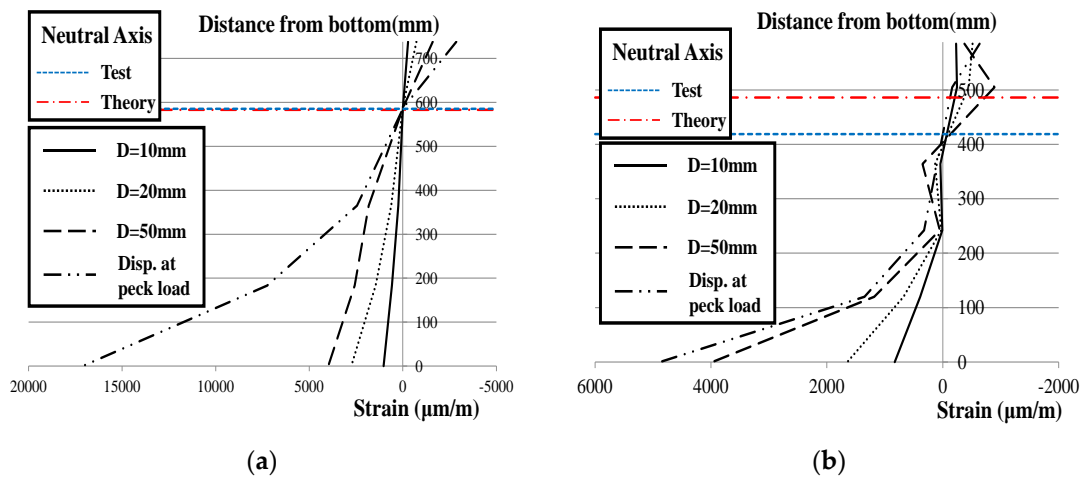


Figure 17. Measured strain distributions of the fully composite specimens: (a) 738-WFC-X-X-TD; (b) 585-TFC-O-R1-DD.

Table 13. Locations of neutral axis at failure of the fully composite specimens.

Specimen	Location of Neutral Axis at Failure (mm)		Ratio of (2) to (1) (%)
	Theory ⁽¹⁾	Test ⁽²⁾	
738-WFC-X-X-TD	154.9	152.6	98.5
585-TFC-O-R1-DD	98.8	166.3	168.3

5. Conclusions

In this study, we proposed a new steel concrete composite beam that has a similar shape to the conventional steel wide flange beam, but whose lower flange has a tubular shape with infilled concrete. The bending capacity of the new composite beam was investigated by performing a two-point loading test on seven specimens, which can be categorized mainly into two types, non-composite and fully

composite specimens. The load versus displacement curves were plotted for all the specimens and their failure modes were identified. Theoretical equations to estimate the flexural strengths of the new composite beam members were proposed and their accuracy was examined by comparing the predictions of the equations with the test results. The main conclusions of this paper are as follows:

- (1) The proposed composite beam with lower tubular flange can have almost equal flexural strength to that of a composite beam with a conventional wide flange at the fully composite stage, although the latter has an almost 26% higher total depth. Consequently, the proposed composite beam is highly effective in reducing the floor height.
- (2) The nominal flexural strength of the proposed composite beam at fully composite stage can be determined based on its plastic moment. The theoretical estimations based on this assumption predicted the experimental results well.
- (3) The nominal flexural strength of the proposed composite beam at the construction stage can be determined based on its yield moment since its ultimate failure mode was generally local web buckling. However, if it does not have any openings in the web, its plastic moment can be taken as the nominal flexural strength, and it is highly resistant to lateral torsional buckling due to the existence of the lower tubular flange.

Acknowledgments: The first author of this paper acknowledges support from NI Steel Co., Ltd. and the Basic Science Research Program through the National Research Foundation of Korea (Grant Number: NRF-2016 R1D1A1B01010615).

Author Contributions: In this paper, Bong Ho Cho and Young-Ho Kim proposed the main concept of the new composite beam; Bong Ho Cho prepared the experimental program to investigate its flexural capacity and made a contribution to the implementation of the experimental program. Jae-Sub Lee analyzed the test results and prepared the tables and figures included in the paper; Dae-Jin Kim derived all of the theoretical flexural strength equations of the new composite beam and wrote the entire manuscript.

Conflicts of Interest: The authors declare no conflict of interest.

References

1. Lu, X.; Mäkeläinen, P. Slim floor developments in Sweden and Finland. *Struct. Eng. Int.* **1996**, *6*, 127–129. [[CrossRef](#)]
2. Lawson, R.M.; Beguin, P.; Obiala, R.; Braun, M. Slim-floor construction using hollow-core and composite decking systems. *Steel Constr.* **2015**, *8*, 85–89. [[CrossRef](#)]
3. Lam, D.; Dai, X.; Kuhlmann, U.; Raichle, J.; Braun, M. Slim-floor construction—design for ultimate limit state. *Steel Constr.* **2015**, *8*, 79–84. [[CrossRef](#)]
4. De Nardin, S.; El Debs, A.L. Composite connections in slim-floor system: An experimental study. *J. Constr. Steel Res.* **2012**, *68*, 78–88. [[CrossRef](#)]
5. De Nardin, S.; El Debs, A.L. Study of partially encased composite beams with innovative position of stud bolts. *J. Constr. Steel Res.* **2009**, *65*, 342–350. [[CrossRef](#)]
6. Lawson, R.M.; Derek, L.M.; Rackham, J.W. *Design of Asymmetric Slimflor Beams Using Deep Composite Decking*; Steel Construction Institute: Ascot, UK, 1997.
7. Braun, M.; Hechler, O.; Birarda, V. 140 m² Column Free Space due to Innovative Composite Slim Floor Design. In Proceedings of the 9th International Conference on Steel Concrete Composite and Hybrid Structures, Leeds, UK, 2009; pp. 978–981.
8. Braun, M.; Hechler, O.; Hauf, G.; Kuhlmann, U. Embodied Energy Optimization by Innovative Structural Systems. Available online: http://sections.arcelormittal.com/uploads/tx_abdownloads/files/Embodied_energy_optimization_by_innovative_structural_system.pdf (accessed on 23 November 2016).
9. Lee, C.H.; Park, H.G.; Park, C.H.; Hwang, H.J.; Lee, C.N.; Kim, H.S.; Kim, S.B. Cyclic seismic testing of composite concrete-filled U-shaped steel beam to H-shaped column connections. *J. Struct. Eng.* **2012**, *139*, 360–378. [[CrossRef](#)]
10. Lee, C.H.; Soh, H.J.; Park, C.H.; Lee, C.N.; Lee, S.H.; Oh, H.N. Flexural Behavior and Design of Concrete-filled U-shape Hybrid Composite Beams Fabricated from 570 MPa High-strength Steel. *J. Korean Soc. Steel Constr.* **2016**, *28*, 109–120. (In Korean) [[CrossRef](#)]

11. Kim, S.B.; Kim, S.S.; Lee, W.R.; Kim, J.Y.; Lee, S.B.; Yoo, D.S.; Kim, D.H. Study on the Flexible Strength of U-shape Hybrid Composite Beam. *J. Korean Soc. Steel Constr.* **2012**, *24*, 521–534. (In Korean) [[CrossRef](#)]
12. Kim, S.B.; Cho, S.H.; Oh, K.S.; Jeon, Y.H.; Choi, Y.H.; Kim, S.S. Bending Performance Evaluation of Hybrid Composite Beam with Low Depth and New Shape. *J. Korean Soc. Steel Constr.* **2016**, *28*, 151–162. (In Korean) [[CrossRef](#)]
13. ASTM Standard C39/C39M-11. *Standard Test Method for Compressive Strength of Cylindrical Concrete Specimens*; Annual Book ASTM Standards: West Conshohocken, PA, USA, 2011.
14. Architectural Institute of Korea (AIK). *Korea Building Code*; AIK: Seoul, Korea, 2009.
15. ASTM Standard A370-12a. *Standard Test Methods and Definitions for Mechanical Testing of Steel Products*; Annual Book ASTM Standards: West Conshohocken, PA, USA, 2012.
16. American Institute of Steel Construction (AISC). *Manual of Steel Construction: Load & Resistance Factor Design*, 2nd ed.; American Institute of Steel Construction: Chicago, IL, USA, 1994.



© 2017 by the authors; licensee MDPI, Basel, Switzerland. This article is an open access article distributed under the terms and conditions of the Creative Commons Attribution (CC-BY) license (<http://creativecommons.org/licenses/by/4.0/>).